Journal of Materials Chemistry A

COMMUNICATION

View Article Online
View Journal | View Issue

Cite this: J. Mater. Chem. A, 2014, 2, 13795

Received 5th May 2014
Accepted 18th June 2014

DOI: 10.1039/c4ta02254h

www.rsc.org/MaterialsA

A 3D hybrid of layered MoS_2/nitrogen-doped graphene nanosheet aerogels: an effective catalyst for hydrogen evolution in microbial electrolysis cells†

Yang Hou,‡[a] Bo Zhang,‡[b] Zhenhai Wen,[a] Shumao Cui,[a] Xiaoru Guo,[a] Zhen He*[c] and Junhong Chen*[a]

Cost-effective catalysts are the key to the successful deployment of microbial electrolysis cells (MECs) for hydrogen production from organic wastes. Herein, we report a novel catalyst for hydrogen evolution in MECs based on a 3D hybrid of layered MoS_2/nitrogen-doped graphene nanosheet aerogels (3D MoS_2/N-GAs) that were prepared by a facile hydrothermal approach. A high output current density of 0.36 mA cm^{-2} with a hydrogen production rate of 0.19 m^3 H_2 m^{-3} d^{-1} was achieved for the hybrid at a 0.8 V bias, significantly higher than that of MoS_2 nanosheets and N-GAs alone and comparable to that of the Pt/C catalyst when being applied in MECs. The outstanding performance of the hybrid benefits from its 3D conductive networks, porous structure, and strong synergic effects between MoS_2 nanosheets and N-GAs, making it a promising catalyst for hydrogen production from wastewater through bio-electrochemical reactions.

Microbial electrolysis cells (MECs) are bio-electrochemical devices in which electrogenic bacteria oxidize organic matter and transfer the generated electrons to a cathode to reduce protons for hydrogen production.[1–6] The energy barrier of proton reduction needs to be overcome with the aid of a catalyst, and Pt-based materials have been the most effective cathode catalysts for MECs;[7] however, high cost and low-abundance hinder the use of Pt catalysts for developing large-scale MEC systems. It is thus attractive to develop cost-effective alternatives that are suitable for MECs; a few successful examples are bulk MoS_2,[8] N-Fe/Fe_3C@C,[3] stainless steel,[9] nickel alloys,[10] and carbon felt[11] materials. Recently, layer-structured MoS_2 has attracted significant interest due to its unique two-dimensional (2D) structure and excellent electrocatalytic activity for hydrogen production.[8,12–14] It has been considered as a promising alternative for Pt-based catalysts. However, poor intrinsic conductivity of MoS_2 limits the overall electrocatalytic performance.[15,16] The most effective pathway to address the above issues is to combine layered MoS_2 with 2D graphene or its derivatives.[17,18] Within the graphene family, nitrogen-doped graphene (NG) is one of the promising candidates because of its excellent electrical conductivity, high chemical stability, and moderate catalytic activity for hydrogen evolution.[19,20] More importantly, the matching layer structure between layered MoS_2 and NG not only increases the contact area for efficient charge transfer across the interface, but also shortens the charge transport time and distance,[21] thereby improving the electrocatalytic activity.

Because the properties of catalysts are dependent on both their composition and structures, the assembly of 2D nanosheets into 3D framework architectures may open up new opportunities for further enhancing catalytic properties because of their rich porosity, large surface area, and excellent network structures compared with 1D or 2D materials.[22–24] Graphene-based aerogels are highly porous 3D carbon materials with an interconnected structure, large open pores, and good electrical conductivity that have wide applications in many fields such as batteries and catalysis.[25,26] Thus, it is anticipated that using graphene-based aerogels as a loading matrix would improve the activity of the embedded electrocatalysts. To the best of our knowledge, there has been no report on controllable synthesis of 3D layered MoS_2/NG nanosheet aerogels (3D MoS_2/N-GAs) as a catalyst for hydrogen production in MECs.

Herein, we report for the first time a facile approach to synthesize a novel 3D MoS_2/N-GA hybrid as an active electrocatalyst for hydrogen production in MECs. Benefiting from its large surface area, porous structure, and high electrical conductivity, this hybrid exhibits significantly enhanced catalytic activity for bio-electrochemical hydrogen evolution that outperforms both bare MoS_2 nanosheets (MoS_2-NS) and N-GAs alone.

[a]Department of Mechanical Engineering, University of Wisconsin-Milwaukee, 3200 North Cramer Street, Milwaukee, Wisconsin 53211, USA. E-mail: jhchen@uwm.edu
[b]Key Laboratory of Environmental Biotechnology, Research Center for Eco-Environmental Sciences, Chinese Academy of Science, Beijing 100085, China
[c]Department of Civil and Environmental Engineering, Virginia Polytechnic Institute and State University, Blacksburg, VA 24061, USA. E-mail: zhenhe@vt.edu

† Electronic supplementary information (ESI) available: See DOI: 10.1039/c4ta02254h

‡ These authors have contributed equally.

Scheme 1 illustrates the preparation procedure for the 3D MoS_2/N-GA hybrid. First, MoS_2-NS was fabricated through a liquid exfoliation process using layered MoS_2 as the precursor. Subsequently, the resulting MoS_2-NS was mixed with graphene oxide (GO) and ammonia dispersions, and then the ternary mixture was hydrothermally assembled to form a 3D MoS_2/N-GA hybrid (details in the Experimental section). In this way, the MoS_2-NS was encapsulated and anchored on graphene nanosheets with the simultaneous reduction of GO and the incorporation of nitrogen species into the graphene framework.

Fig. 1a shows a digital image of the monolithic 3D MoS_2/N-GA hybrid. The morphology of the 3D hybrid architecture is similar to those reported for graphene and GO aerogels.[27] A typical field emission scanning electron microscopy (FESEM) image of N-GAs shows that a well defined and interconnected 3D porous N-GA network with continuous macropores of several-hundred nanometers in diameter was clearly discerned (Fig. 1b). The porous networks would favor mass transfer and reduce transport limitation of the electrolyte at the cathode. After the formation of 3D MoS_2/N-GA architecture, the thin and rigid MoS_2-NS was grown within the N-GA networks (Fig. 1c), which can efficiently prevent the aggregation and restacking of MoS_2-NS; no apparent aggregates appeared. Since the graphene-like morphology of the 3D MoS_2/N-GA hybrid makes it difficult to distinguish MoS_2-NS and N-GAs, energy dispersive X-ray (EDX) spectroscopy was carried out (inset of Fig. 1c). The results revealed that main elements of the hybrid are Mo, S, C, N and O, which further confirms the formation of MoS_2-NS inside the 3D N-GA network. The content of MoS_2-NS (29.0 wt%) in the 3D MoS_2/N-GA hybrid was confirmed by thermogravimetric analysis (TGA) (Fig. S1†).

Further insights into the morphology of the hybrid were obtained from transmission electron microscopy (TEM) and high-resolution TEM (HRTEM) images. The 3D MoS_2/N-GA hybrid displayed laminar structured MoS_2 (black stripes) dispersed on the surface of the crumpled NG sheets (Fig. 1d). The corresponding selected area electron diffraction (SAED) pattern presented several diffraction rings, which can be well indexed to the planes of hexagonal-phase MoS_2 and N-GAs sheets (inset of Fig. 1e).[21] The HRTEM images of the hybrid show that the layered MoS_2 (4–7 layers) with a lattice spacing of 0.63 nm was dispersed on the surface of the N-GA sheets (Fig. 1e and f). Atomic force microscopy (AFM) indicated that MoS_2 had a 2D nanosheet structure and the typical thickness was about 5.83 nm, which agree well with the 9-layer MoS_2-NS (Fig. S2†).[28] In addition, the thickness of the N-GA nanosheets was about 1 nm, which corresponds to 3 layers of graphene based on the theoretical thickness of a single-layer of graphene (~0.34 nm). Importantly, the HRTEM image also shows a distinguished and coherent interface between the MoS_2-NS and N-GAs (Fig. 1f), indicating that an intimate contact might be formed, which could result in more efficient electron transfer within the hybrid and improve the overall catalytic activity for MECs.

The XRD patterns of the 3D MoS_2/N-GA hybrid (Fig. S3†) indicate that GO has been reduced to NG nanosheets after the hydrothermal treatment and that the MoS_2-NS was in the form of hexagonal crystal structures (JCPDS 37-1492). The results confirmed the co-existence of MoS_2-NS and N-GAs. X-ray photoelectron spectroscopy (XPS) revealed the presence of Mo,

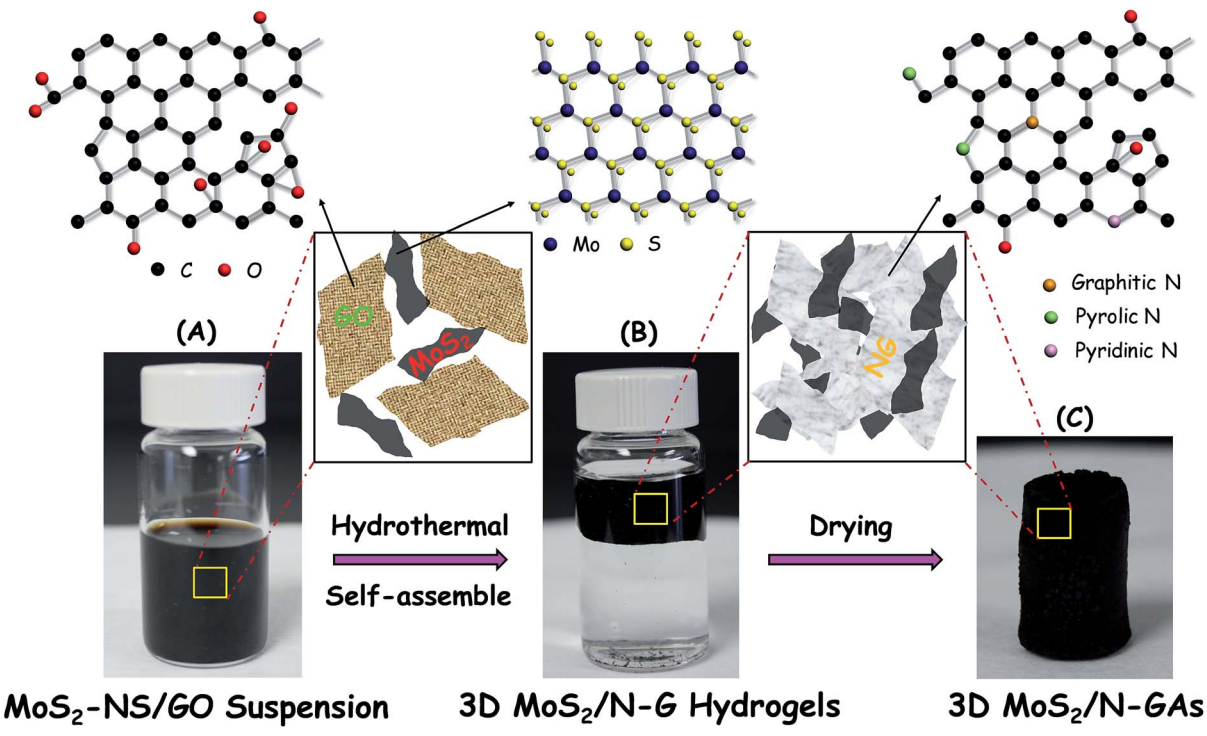

Scheme 1 Schematic illustration of the synthesis process of 3D MoS_2/N-GAs.

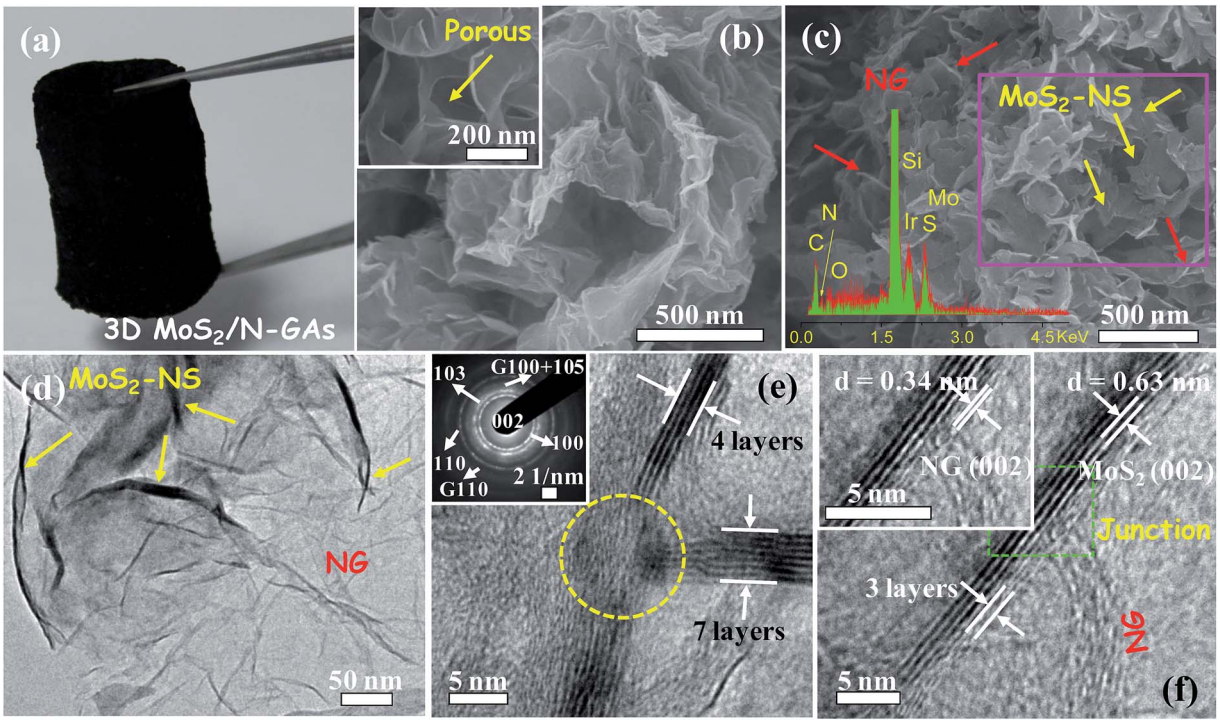

Fig. 1 Photograph of 3D MoS_2/N-GAs (a). FESEM images of N-GAs (b) and 3D MoS_2/N-GAs (c). The inset of (b) shows the high magnification FESEM image of N-GAs; the inset in (c): the corresponding EDX spectrum of 3D MoS_2/N-GAs. (d–f) TEM and HRTEM images of 3D MoS_2/N-GAs. The inset in (e) is the corresponding SAED pattern. The inset in (f) shows the lattice spacing of 3D MoS_2/N-GAs.

S, C, N, and O elements in the 3D MoS_2/N-GA hybrid with a Mo/S atomic ratio of ~1 : 2, which is in good agreement with the theoretical value of MoS_2 (Fig. S4a†). The Mo 3d and S 2p spectra can be fitted by two spin-orbit doublets characteristic of Mo^{4+} and S^{2-}, respectively (Fig. S4b and S4c†).[21] For the high-resolution XPS spectrum of N 1s (Fig. S5†), it is difficult to distinguish the N 1s signal from N-doping or the presence of MoS_2 because the N 1s peak overlapped with the strong Mo $2p_{3/2}$ signal. However, the N 1s peak can be clearly observed from the 3D hybrid without MoS_2-NS loading (Fig. S6†). Considering that the presence of MoS_2 has almost no effect on N-doping during the hydrothermal process,[29] one can draw the conclusion that the N-atoms have been successfully incorporated into the 3D MoS_2/N-GA hybrid. In addition, the results of the C 1s XPS spectrum confirmed the reduction of GO and the successful nitrogen doping in the 3D hybrid (Fig. S7†). Raman spectra show that the 3D MoS_2/N-GA hybrid has two distinct bands at 378 and 403 cm^{-1}, which belong to the E_{2g} and A_{1g} modes of MoS_2, respectively (Fig. S8†).[30] The characteristic disorder-induced D and graphitic-G bands of graphene are observed at 1334 and 1591 cm^{-1}, respectively, indicating the presence of graphene in the hybrid. The apparent increase in the I_D/I_G ratios from GO (0.99) to the 3D MoS_2/N-GA hybrid (1.03) confirms the successful conversion of GO to N-GAs with more disorderly stacked graphene sheets.[31] Moreover, the downshift of the G peak from GO (1604 cm^{-1}) to RGO (1599 cm^{-1}) can be attributed to the restoration of the conjugated structure.[32] The further downshift of the G peak in the 3D MoS_2/N-GA hybrid (1591 cm^{-1}) may be related to the incorporation of N heteroatoms.[33] Previous studies showed that the substitution of carbon atoms with nitrogen could cause n-type doping, resulting in the down-shift of the G band.[34] The above results provide evidence for the incorporation of N atoms into graphene. The nitrogen adsorption–desorption isotherm (Fig. S9†) of the 3D MoS_2/N-GA hybrid indicates that it possesses a typical mesoporous structure and that the Brunauer–Emmett–Teller (BET) surface area is about 43 $m^2\ g^{-1}$, with an average pore size of 71 nm, which is essential for diffusion of the electrolyte and increasing contact between the electrolyte and the catalyst.[35]

The electrocatalytic activity of the 3D MoS_2/N-GA hybrid toward the hydrogen evolution reaction (HER) was investigated in neutral media (100 mM phosphate buffer solution (PBS)) by linear sweep voltammetry using a three-electrode setup (Fig. 2a). The 3D MoS_2/N-GA hybrid exhibited a small onset overpotential of 236 mV toward the HER (all electrochemical potentials reported herein are relative to a reversible hydrogen electrode (RHE)), beyond which the cathodic current rose rapidly under more negative potentials. In contrast, both MoS_2-NS and N-GAs showed much less HER activity, with onset potentials of 337 and 495 mV, respectively, indicating that both the 3D N-GAs and MoS_2-NS are important to enhance the electrocatalytic activity for the HER. Additionally, the hybrid exhibited a high current density of 40.7 mA cm^{-2} at −0.4 V, which was much higher than those observed for MoS_2-NS (11.4 mA cm^{-2}) and N-GAs (4.9 mA cm^{-2}), although it was lower than the commercial Pt/C catalyst (10% Pt on Vulcan XC-72) at the same potential. Moreover, the overpotentials required for the 3D MoS_2/N-GA hybrid to produce cathodic current densities

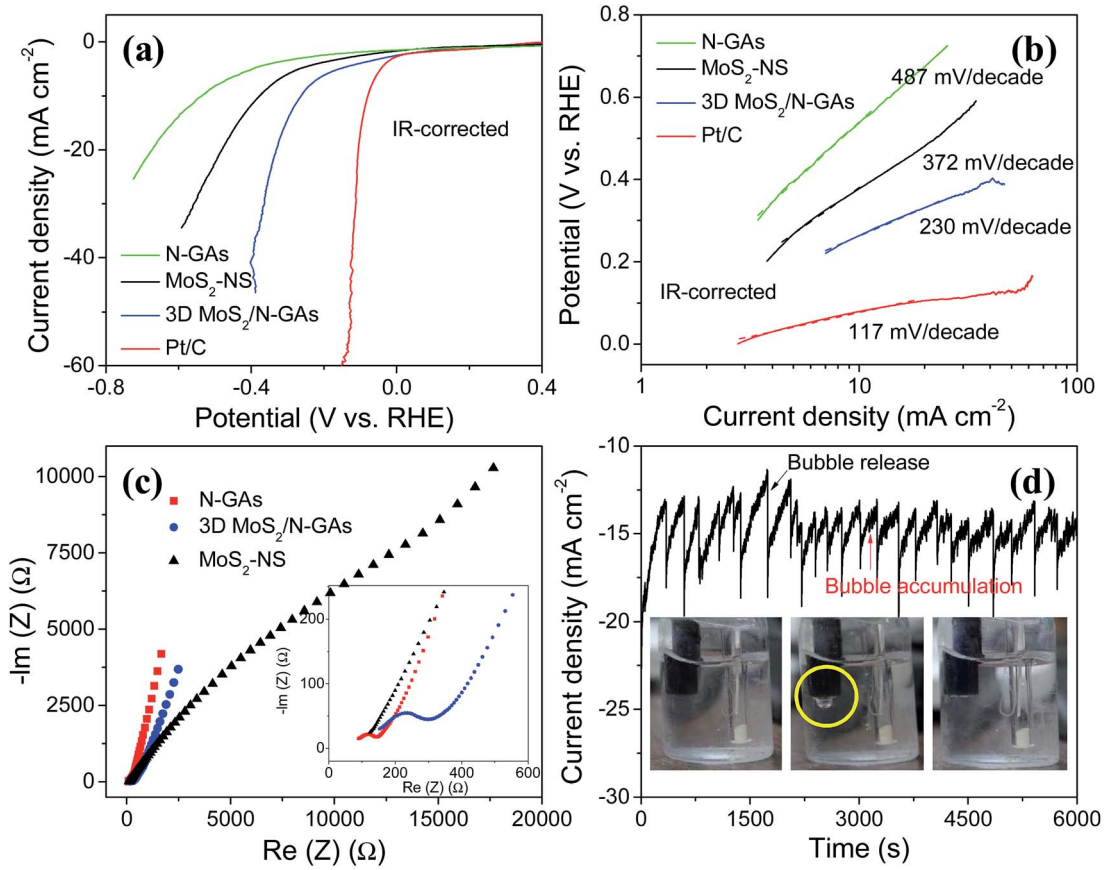

Fig. 2 (a) Polarization curves, (b) corresponding Tafel plots, and (c) EIS Nyquist plots of MoS_2-NS, N-GAs, 3D MoS_2/N-GAs, and Pt/C at 5 mV s^{-1} in 100 mM PBS. The iR drop was corrected. (d) Time dependence of cathodic current density during electrolysis at −0.3 V.

of 10 and 5 mA cm^{-2} were 261 and 167 mV, respectively. These overpotentials compared favorably with some of the best non-noble metal HER catalysts for neutral media that have been reported to date. For example, amorphous molybdenum sulfide showed a lower current density of 5 mA cm^{-2} at ~370 mV,[36] and electrodeposited cobalt-sulfide required an overpotential of ~120 mV for HER.[37] Moreover, cobalt-embedded nitrogen-rich carbon nanotubes gave a current density of 10 mA cm^{-2} at 540 mV.[38]

Due to the HER's inherently slow kinetics under neutral media,[39] a relatively small Tafel slope of 230 mV per decade was observed for the 3D MoS_2/N-GA hybrid, but it was much smaller than the values obtained for MoS_2-NS and N-GAs, which were 372 and 487 mV per decade, respectively (Fig. 2b). For practical applications, a small Tafel slope is desirable as it will enable a faster increase of the HER rate with increasing overpotentials. The low Tafel slope of the 3D MoS_2/N-GA hybrid may be attributed to the strong electronic coupling between MoS_2-NS and N-GAs, permitting efficient electron transport from the active sites to the underlying electrode substrate. This hypothesis was further confirmed by electrochemical impedance spectroscopy (EIS). The 3D MoS_2/N-GA hybrid showed a smaller semicircle than did the MoS_2-NS (Fig. 2c), suggesting a smaller charge transfer resistance in the 3D MoS_2/N-GA hybrid,[40] likely due to the introduction of N-GAs that enhance the electrical conductivity of the 3D MoS_2/N-GA hybrid and decrease the electron transfer resistance between MoS_2-NS. This reduced resistance implies much faster HER kinetics with the 3D MoS_2/N-GA hybrid.[41] After a long period of 6000 s, only a slight decrease in the current density was observed for the 3D MoS_2/N-GA hybrid, suggesting superior stability (Fig. 2d). The slow decline may be due to the continuous consumption of H^+ and the potential loss of the dropcast material from the surface of the electrode.[42] Moreover, the typical serrate shape can be attributed to the alternating processes of H_2 bubble accumulation and release.[43]

To further evaluate the performance of the hybrid in MECs, we compared the current generation and hydrogen production of different electrodes. When applying 0.8 V to the MECs, an electric current was generated that was directly related to bio-electrochemical hydrogen production *via* electron transfer. Fig. 3a shows the current generation in MECs when different catalysts were employed. The MECs with the 3D MoS_2/N-GA hybrid generated a peak current density of 0.36 mA cm^{-2}, which was about 1.29 and 1.44 times greater than those of MoS_2-NS (0.28 mA cm^{-2}) and N-GAs (0.25 mA cm^{-2}), respectively, and close to that of the Pt/C catalyst (0.40 mA cm^{-2}). Moreover, the MEC with 3D MoS_2/N-GAs exhibited higher cathodic efficiencies as well (Table S1†). Combining these results, it was confirmed

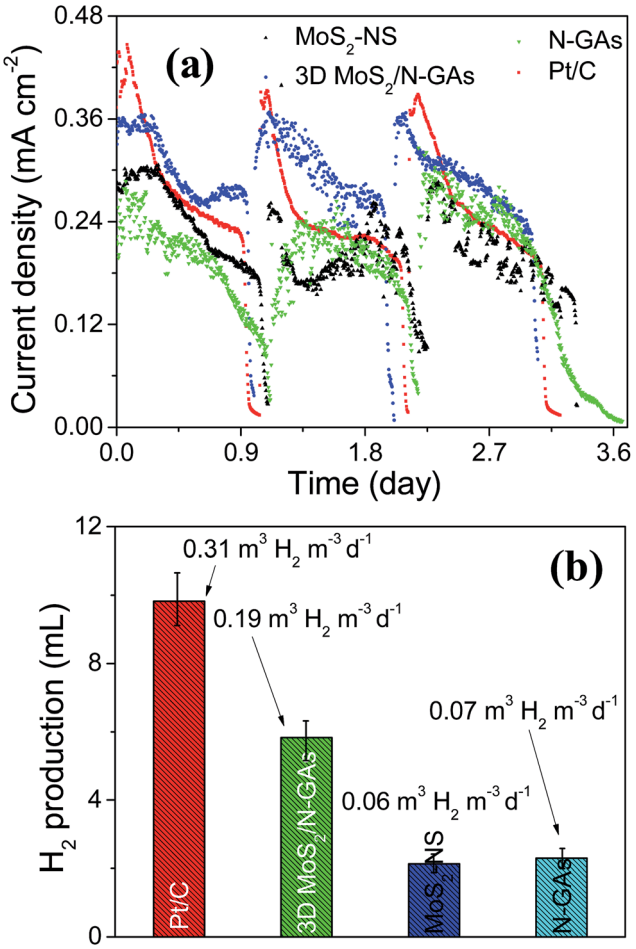

Fig. 3 (a) Current generation and (b) hydrogen production with MoS_2-NS, N-GAs, 3D MoS_2/N-GAs, and Pt/C cathodes in the MECs at an external resistor of 1 Ω and an applied voltage of 0.8 V.

that the hybrid catalyst had a higher catalytic activity towards the HER than did MoS_2-NS and MoS_2/N-GAs alone.

As a result of the higher current density and cathodic efficiency, the hydrogen production rate of 0.19 m^3 H_2 m^{-3} d^{-1} was observed in the 3D MoS_2/N-GA hybrid MEC (Fig. 3b). This rate exceeded those obtained with MoS_2-NS alone and N-GAs alone by more than 3.17 and 2.71 times, respectively. Although the 3D MoS_2/N-GA hybrid (43 m^2 g^{-1}) had a smaller BET surface area than N-GAs (83 m^2 g^{-1}), the catalytic activity of the hybrid was much higher than the N-GAs, further confirming that the structure of the hybrid catalyst gave it excellent catalytic performance. Additionally, visual observation and photography confirm the formation of bubbles on the cathode, suggesting the hydrogen production from the MECs (Fig. S10†).

Even though the loading rate of the 3D MoS_2/N-GAs was roughly $1/4^{th}$ that of the Pt/C catalyst and the surface area was $1/5^{th}$ of it, the 3D MoS_2/N-GA hybrid reached a peak current level almost the same as the Pt/C catalyst. However, due to a lower cathodic efficiency, the MEC with the 3D MoS_2/N-GA hybrid catalyst generated less hydrogen than the MEC with the Pt/C catalyst did. Notably, the hybrid possessed the highest Coulombic efficiency of ~24.28% among the four samples tested (Table S1†). The increased MEC performance with the hybrid is obvious when compared with the MoS_2-NS and N-GAs. We believe that the high electrocatalytic activity for MECs originated from synergic effects within the aerogel structure with large surface areas, layered MoS_2 for abundant catalytic active sites, and 3D N-GAs networks for efficient charge transfer, the detailed contributions of which are currently being investigated.

Conclusions

In summary, we have designed and fabricated a novel 3D MoS_2/N-GA hybrid using a facile two-step method through self-assembly of a mixture of GO and MoS_2-NS in the presence of an ammonia solution for high-performance bio-cathode materials in MECs. Benefiting from the unique structure, the hybrid exhibited a large output current density, a high hydrogen production rate, and excellent cycling stability, superior to those of individual MoS_2-NS and N-GAs. This work provides fundamental insights for further design and construction of other 3D layered hybrid aerogel catalysts for bio-electrochemical hydrogen evolution in MECs.

Acknowledgements

Financial support for this work was provided by the U.S. Department of Energy (DE-EE0003208) and the Research Growth Initiative Program of the University of Wisconsin-Milwaukee (UWM).

Notes and references

1 A. W. Jeremiasse, H. V. M. Hamelers, M. Saakes and C. J. N. Buisman, *Int. J. Hydrogen Energy*, 2010, **35**, 12716–12723.
2 Y. Kim and B. E. Logan, *Proc. Natl. Acad. Sci. U. S. A.*, 2011, **108**, 16176–16181.
3 L. Xiao, Z. Wen, S. Ci, J. Chen and Z. He, *Nano Energy*, 2012, **1**, 751–756.
4 M. Sun, G. P. Sheng, L. Zhang, C. R. Xia, Z. X. Mu, X. W. Liu, H. L. Wang, H. Q. Yu, R. Qi, T. Yu and M. Yang, *Environ. Sci. Technol.*, 2008, **42**, 8095–8100.
5 A. W. Jeremiasse, H. V. M. Hamelers and C. J. N. Buisman, *Bioelectrochemistry*, 2010, **78**, 39–43.
6 B. E. Logan, D. Call, S. Cheng, H. V. M. Hamelers, T. H. J. A. Sleutels, A. W. Jeremiasse and R. A. Rozendal, *Environ. Sci. Technol.*, 2008, **42**, 8630–8640.
7 J. Y. Nam, R. D. Cusick, Y. Kim and B. E. Logan, *Environ. Sci. Technol.*, 2012, **46**, 5240–5246.
8 J. C. Tokash and B. E. Logan, *Int. J. Hydrogen Energy*, 2011, **36**, 9439–9445.
9 D. F. Call, M. D. Merrill and B. E. Logan, *Environ. Sci. Technol.*, 2009, **43**, 2179–2183.
10 P. A. Selembo, M. D. Merrill and B. E. Logan, *J. Power Sources*, 2009, **190**, 271–278.
11 H. S. Lee, C. I. Torres, P. Parameswaran and B. E. Rittmann, *Environ. Sci. Technol.*, 2009, **43**, 7971–7976.

12 H. I. Karunadasa, E. Montalvo, Y. Sun, M. Majda, J. R. Long and C. J. Chang, *Science*, 2012, **335**, 698–702.
13 T. F. Jaramillo, K. P. Jorgensen, J. Bonde, J. H. Nielsen, S. Horch and I. Chorkendorff, *Science*, 2007, **317**, 100–102.
14 D. Merki and X. Hu, *Energy Environ. Sci.*, 2011, **4**, 3878.
15 J. Xie, J. Zhang, S. Li, F. Grote, X. Zhang, H. Zhang, R. Wang, Y. Lei, B. Pan and Y. Xie, *J. Am. Chem. Soc.*, 2013, **135**, 17881–17888.
16 M. A. Lukowski, A. S. Daniel, F. Meng, A. Forticaux, L. Li and S. Jin, *J. Am. Chem. Soc.*, 2013, **135**, 10274–10277.
17 F. Meng, J. Li, S. K. Cushing, M. Zhi and N. Wu, *J. Am. Chem. Soc.*, 2013, **135**, 10286–10289.
18 U. Maitra, U. Gupta, M. De, R. Datta, A. Govindaraj and C. N. R. Rao, *Angew. Chem., Int. Ed.*, 2013, **52**, 13057–13061.
19 H. Wang, T. Maiyalagan and X. Wang, *ACS Catal.*, 2012, **2**, 781–794.
20 L. Qu, Y. Zhao, C. Hu, L. Song, L. Wang, G. Shi and L. Dai, *Energy Environ. Sci.*, 2014, **7**, 1913–1918.
21 Y. Hou, Z. Wen, S. Cui, X. Guo and J. Chen, *Adv. Mater.*, 2013, **25**, 6291–6297.
22 Z. S. Wu, S. Yang, Y. Sun, K. Parvez, X. Feng and K. Müllen, *J. Am. Chem. Soc.*, 2012, **134**, 9082–9085.
23 Y. Gong, S. Yang, Z. Liu, L. Ma, R. Vajtai and P. M. Ajayan, *Adv. Mater.*, 2013, **25**, 3979–3984.
24 J. Biener, M. Stadermann, M. Suss, M. A. Worsley, M. M. Biener, K. A. Rose and T. F. Baumann, *Energy Environ. Sci.*, 2011, **4**, 656–667.
25 W. Chen, S. Li, C. Chen and L. Yan, *Adv. Mater.*, 2011, **23**, 5679–5683.
26 H. P. Cong, X. C. Ren, P. Wang and S. H. Yu, *ACS Nano*, 2012, **6**, 2693–2703.
27 C. Li and G. Shi, *Adv. Mater.*, 2014, **26**, 3992–4012.
28 H. Li, X. Qi, J. Wu, Z. Zeng, J. Wei and H. Zhang, *ACS Nano*, 2013, **7**, 2842–2849.
29 K. Chang, D. Geng, X. Li, J. Yang, Y. Tang, M. Cai, R. Li and X. Sun, *Adv. Energy Mater.*, 2013, **3**, 839–844.
30 Y. Li, H. Wang, L. Xie, Y. Liang, G. Hong and H. Dai, *J. Am. Chem. Soc.*, 2011, **133**, 7296–7299.
31 Y. Hou, F. Zuo, A. Dagg and P. Feng, *Nano Lett.*, 2012, **12**, 6464–6473.
32 K. N. Kudin, B. Ozbas, H. C. Schniepp, R. K. Prud'homme, I. A. Aksay and R. Car, *Nano Lett.*, 2007, **8**, 36–41.
33 Z. Lin, G. Waller, Y. Liu, M. Liu and C. P. Wong, *Adv. Energy Mater.*, 2012, **2**, 884–888.
34 H. L. Guo, P. Su, X. Kang and S. K. Ning, *J. Mater. Chem. A*, 2013, **1**, 2248–2255.
35 H. Yin, C. Zhang, F. Liu and Y. Hou, *Adv. Funct. Mater.*, 2014, **24**, 2930–2937.
36 D. Merki, S. Fierro, H. Vrubel and X. Hu, *Chem. Sci.*, 2011, **2**, 1262–1267.
37 Y. Sun, C. Liu, D. C. Grauer, J. Yano, J. R. Long, P. Yang and C. J. Chang, *J. Am. Chem. Soc.*, 2013, **135**, 17699–17702.
38 X. Zou, X. Huang, A. Goswami, R. Silva, B. R. Sathe, E. Mikmeková and T. Asefa, *Angew. Chem., Int. Ed.*, 2014, **53**, 4372–4376.
39 H. Vrubel and X. Hu, *Angew. Chem., Int. Ed.*, 2012, **51**, 12703–12706.
40 Y. Hou, F. Zuo, A. P. Dagg, J. Liu and P. Feng, *Adv. Mater.*, 2014, DOI: 10.1002/adma.201401032.
41 Y. Hou, T. Huang, Z. Wen, S. Mao, S. Cui and J. Chen, *Adv. Energy Mater.*, 2014, DOI: 10.1002/aenm.201400337.
42 E. J. Popczun, C. G. Read, C. W. Roske, N. S. Lewis and R. E. Schaak, *Angew. Chem., Int. Ed.*, 2014, **53**, 5427–5430.
43 J. Xie, H. Zhang, S. Li, R. Wang, X. Sun, M. Zhou, J. Zhou, X. W. Lou and Y. Xie, *Adv. Mater.*, 2013, **25**, 5807–5813.

